China Steel Technical Report, No. 37, pp.58－66, (2024)

Development of Finely Reduced Iron Powder (FRIP) for Metal Injection Molding

HUNG-SHANG HUANG, KUN-YANG WU and YEN-CHOU CHEN

New Materials Research & Development Department
China Steel Corporation

Carbonyl iron powder (CIP), produced through the carbonyl decomposition method, is the most commonly used fine spherical iron powder in the metal injection molding (MIM) industry. This paper aims to utilize gaseous reduction (GR) of hematite powder to produce fine iron powder that is also suitable for use in MIM. The porous reduced iron agglomerates produced by the hydrogen reduction of hematite were mechanically pulverized and spheroidized (MPS). The surface of the iron powder treated with MPS was further coated with silica through sol-gel coating (SGC) to create nanoscale roughness. Through the combination and optimization of the three processes (GR+MPS+SGC), we were able to achieve finely reduced iron powders (FRIP) that are nearly spherical. The D50 particle size was approximately 5 μm, and the tap density exceeded 4 g/cm³. The FRIP was used to produce Fe-2Ni alloy (MIM-2200) through the MIM process. The kneading behavior, each step of the MIM process, and the sintered properties of Fe-2Ni produced by the FRIP were examined and compared with those of commercial CIP. The results show that the silica-coated FRIP exhibited good kneading ability and formed a suitable feedstock for injection molding. After sintering, the Fe-2Ni alloy produced by the FRIP achieved a higher sintered density and superior dimensional stability compared to that produced using the CIP. This indicates that the FRIP has great potential for application in the MIM industry.

Keywords: Finely reduced iron powder, MIM, Tap density, Fe-2Ni

1. INTRODUCTION

Fine spherical iron powder refers to pure iron powder that has a spherical shape and an average particle size smaller than 10 μm. Nowadays, the most commonly used type of fine spherical iron powder is carbonyl iron powder (CIP), which is produced using the carbonyl decomposition method[1, 2]. CIP exhibits several unique features, including small particle size, high packing density, high purity, superior sinterability, and good electromagnetic properties. Therefore, CIP can be widely applied as an industrial raw material in various fields, such as metal injection molding (MIM), magnetic inductors, and microwave/radar absorption. However, the manufacturing of CIP is costly and is accompanied by a high risk of industrial safety hazards. The complexity of carbonyl decomposition arises from the series of steps involved, including carbonyl synthesis, distillation, purification, and thermal decomposition. This process involves the reaction of carbon monoxide, a colorless, odorless, but poisonous gas, with iron under specific conditions of high pressure and temperature. The result is the formation of iron pentacarbonyl ($Fe(CO)_5$), which is an intermediate product that is also highly toxic. To reduce industrial safety accidents, it is necessary to introduce high-quality manufacturing equipment and safety assurance devices that can ensure safe and secure operation in high-temperature, high-pressure, and airtight environments. Therefore, the initial investment cost is high, and consequently, the market price of CIP is relatively high. If a new cost-effective method for producing fine spherical iron powder with relatively low industrial safety risks is developed, it has the potential to enter the MIM and other application markets.

The characteristic of the iron powder prepared by the gaseous reduction (GR) method is the formation of an irregular, coarse iron powder, commonly known as sponge iron powder, which contains numerous pores[3]. A coarse, porous sponge iron powder can be characterized as a form of iron powder with both a coarse texture and a porous structure, formed through the presintering of numerous fine iron powders. At this stage, the introduction of the mechanical pulverizing and spheroidizing (MPS) method offers the potential to produce fine iron powder with a small particle size and a nearly spherical shape. Such a notion has been suggested in some previous studies. For instance, Clark et al.[4] proposed using Fe_2O_3 iron oxide powder with a particle size of less than 1000 μm as the raw material. The iron oxide powder was initially ground to achieve an average particle size of

less than 20 μm. The iron oxide powder was then introduced into a reducing atmosphere within a specific temperature range to obtain reduced iron. Afterward, it was finely ground using jet mill equipment. Finally, a fine iron powder with particle sizes of D10/D50/D90 = 1.8/2.7/3.9 μm and a tap density of approximately 2.8 g/cm³ can be obtained. Its sinterability is better than that of CIP.

Walther et al.[5, 6] granulated the fine Fe_2O_3 iron oxide powders (0.2~0.8 μm) to obtain spherical agglomerates and then sieved to a particle size smaller than 32 μm for the following two-stage reduction. The first stage was reduced at 500°C, while the second stage was reduced at 700°C and 850°C, respectively. Finally, the Hybridizer[7], a specialized pulverizing and spheroidizing machine, was used to mill the reduced iron agglomerates to obtain fine iron powders with improved sphericity. As a result, when reduced at 700°C, particle sizes of D10/D50/D90=3.4/5.1/7.6 μm and a tape density of 2.8 g/cm³ can be achieved. When reduced at 850 °C, the iron powders exhibit larger particle sizes with D10/D50/D90=7.3/11.4/16.9 μm and a higher tap density of 3.3 g/cm³. Unlike the approach of Walther et al., Chen et al.[8] did not process the iron oxide powders into granulated powders; instead, they directly reduced the iron oxide powders to form the reduced iron agglomerates. MPS was conducted using an air classifying mill (ACM), a commonly utilized equipment in the industry known for its high feasibility in mass production. They reported that the roundness and tap density of the reduced iron powders can be further improved by conducting two rounds of MPS treatments, with annealing done before the second MPS treatment. Finally, the finely reduced iron powder (FRIP) with a particle size of D50 = 6.5~7.0 μm and a tap density of 3.46~3.48 g/cm³ is obtained.

Although the production of the FRIP by employing GR + MPS has been proposed for some time, it is still rare to see this process being commercialized and used in the MIM market. It is presumed that the powder characteristics of the FRIP are still not yet optimized and cannot meet the requirements for the current MIM application. For instance, metal powders used in MIM typically need to have a high tap density. A high tap density indicates a relatively high amount of metal powder loading in the MIM feedstock, making it easier to achieve high density during sintering [9]. The shrinkage of the sintered part is also relatively low, and the dimensional control is more stable. In addition, powders with a higher tap density generally exhibit good fluidity, which is also beneficial for kneading and injection molding. In the context of the CIP for the MIM industry, the tap density is typically greater than 4 g/cm³. However, the tap densities of the FRIP reported in the previous literature are much lower than this value.

The tap density and fluidity of metal powders are influenced by the particle size, shape, and inter-particle adhesion/cohesion forces. Several studies[10-12] have reported that introducing nano-guest particles into host powders can reduce the adhesion/cohesion force, thereby increasing the fluidity and bulk density of the host powders. Therefore, this study combines the processes of GR, MPS, and the nanoparticle coating of silica on the iron powder surface, to enhance the tap density of FRIP. Furthermore, the suitability of the silica-coated FRIP for application in MIM is being examined.

2. EXPERIMENTAL METHOD

2.1 FRIP Preparation

High-purity hematite powder (Fe_2O_3), a by-product from the hydrochloric acid regeneration plant for recycling pickling line waste in China Steel Corporation, was used as the initial material in this study. Its morphology and characteristics are given in Figure 1 and Table 1, respectively. Figure 2 illustrates the schematic of the preparation of FRIP and the size and shape changes of the iron powder at each stage. First, the hematite powder was placed in a hydrogen atmosphere furnace and heated to 650~850°C for 3 hours for the GR treatment. Thus, the hematite powder is reduced and partially sintered to form agglomerates of reduced iron powder. For the MPS treatment, the iron powder agglomerates were pulverized and spheroidized using ACM. The operating parameters of ACM mainly refer to literature A as the basis and are fine-tuned to achieve the appropriate particle size, shape, and tap density of FRIP. For surface treatment, the FRIP was coated with nano-silica using sol-gel coating (SGC). Tetraethoxysilane (TEOS) was used as the precursor monomer of silica, and ethanol was used as the reaction solvent. More details on the SGC treatment mainly refer to literature[13].

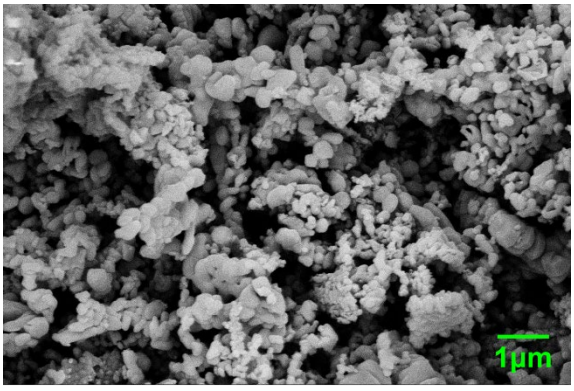

Fig.1. The morphology of the iron oxide powder used in this study.

Table 1 Characteristics of the iron oxide powder used in this study.

Hematite Powder	Characteristics
Grade	Fe_2O_3
Supplier	China Steel Corp.
Particle Size (Fisher sub sieve sizer)	0.83 μm
BET surface area	3.60 m^2/g
Shape	Irregular
Impurities	
Mn,	0.26 wt%
Si,	0.006 wt%
Cl,	0.078 wt%
H_2O,	0.14 wt%

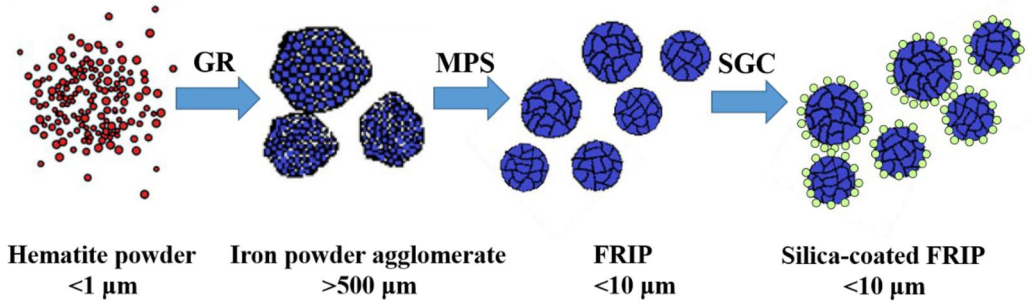

Fig.2. Schematics illustrating the process flow for preparing the finely reduced iron powder (FRIP).

2.2 Characterization and Evaluation for MIM Application

The powder properties of the FRIP and the silica-coated FRIP, including the particle size, tap density, carbon/oxygen/nitrogen (C/O/N) content, and specific surface area (SSA), were measured and compared with two commercial CIP powders (CIP-low carbon and CIP-high carbon, BASF, Germany) that are commonly used in MIM. The particle sizes and size distributions of each iron powder were measured using a laser scattering particle size analyzer (HELOS/BR, Sympatec, Germany). The tape density was measured according to the Metal Powder Industries Federation (MPIF) Standard No. 46 The carbon/sulfur (C/S) analyzer (EMIA-820V, HORIBA, Japan) and the oxygen/nitrogen (O/N) analyzer (EMIA-620W, HORIBA, Japan) were used to measure the carbon, oxygen, and nitrogen content of the iron powders. The SSA was determined using a surface area and porosity analyzer (ASAP 2020, Micromeritics Instrument, USA). The surface morphology and chemical composition of the iron powders were characterized using scanning electron microscopy (SEM, Crossbeam 350, ZEISS, Germany) and transmission electron microscopy (TEM, JEM-2010, JEOL, Japan) equipped with an energy-dispersive X-ray spectrometer (EDS). The silicon content of the silica-coated FRIP was measured using Inductively Coupled Plasma-Optical Emission Spectrometry (ICP-OES 5110, Agilent, USA).

To evaluate the feasibility of our FRIP application in the MIM industry, Fe-2Ni alloy steel (MPIF material name code: MIM-2200), which is a well-known MIM material, was selected as the object for conducting trial production by incorporating FRIP into the MIM process. To prepare the Fe-2Ni feedstock, the FRIP was first mixed with 2 wt% nickel powder (T123TM, Vale, Canada) and then kneaded in a sigma-shaped kneader with varying weight percentages of a multi-component binder. The binder consisted of 40 wt% polyethylene (PE), 55 wt% paraffin wax (PW), and 5 wt% stearic acid (SA). During kneading, we qualitatively assess the uniformity of the mix, its viscosity, and the doughability of the organic/inorganic compounds to determine if the metal powders and binders have been properly blended and transformed into a usable feedstock. After kneading, these feedstocks were molded into rectangular flat specimens of 30x10x3.25 mm using an injection molding machine. To remove the binder, the molded specimens were first immersed in n-Heptane at 45°C for 24 hours to eliminate PW and SA. Subsequently, they were placed in a tube furnace at 650°C for 1 hour in a hydrogen atmosphere for thermal debinding to remove the backbone

binder (PE). Finally, sintering was carried out at 1300°C for 2 hours in a hydrogen atmosphere to complete the trial production of MIM Fe-2Ni steel. The same MIM procedure was also performed for CIP-low carbon and CIP-high carbon as the benchmark for comparison.

The density of the sintered compacts was measured using the Archimedes' method. The hardness was measured using a Rockwell hardness tester (ATK-600, Mitutoyo Corp., Kawasaki, Japan). A vernier scale (500-151-30, Mitutoyo, Japan) with an accuracy of 0.01 mm was used to measure the length and width of the sintered compacts produced by different iron powders and calculate their standard deviation to compare the dimensional stability. The reported data are averages of at least 100 specimens. The oxygen, carbon, and nitrogen contents of the sintered compacts were also measured using the carbon/sulfur (C/S) analyzer and the oxygen/nitrogen (N/O) analyzer. The microstructures were observed using an optical microscope (OM, DMRM, Leica Microsystems Inc., Wetzlar, Germany).

3. RESULTS AND DISCUSSION

3.1 Preparation and Characteristics of FRIP

Figure 3 illustrates the weight loss and changes in oxygen content of the hematite powder reduced in a pure hydrogen atmosphere at various temperatures. Theoretically, hematite contains about 30.06 wt% oxygen content. When reduced at 650°C, the weight loss of the hematite powder was about 29.33 wt%, and the oxygen content dropped to 0.58 wt%, indicating that almost all Fe_2O_3 had been reduced to pure iron. As the reduction temperature increased further, the weight loss gradually increased, and the oxygen content gradually decreased. The higher the reduction temperature, the better the degree of reduction. However, after the temperature reaches above 750°C, the reduction rate gradually decreases. In terms of the morphologies of the reduced iron at different temperatures, Figure 4 shows that reduction at 650°C also caused the original submicron-sized Fe_2O_3 powders to coarsen into micron-sized iron powders and the formation of solid-state necks between iron particles. Moreover, the higher the reduction temperature, the more pronounced the sintering neck becomes, indicating that the reduction process of iron oxide powders is inevitably accompanied by the sintering phenomenon of iron powders. Therefore, the utilization of MPS is necessary.

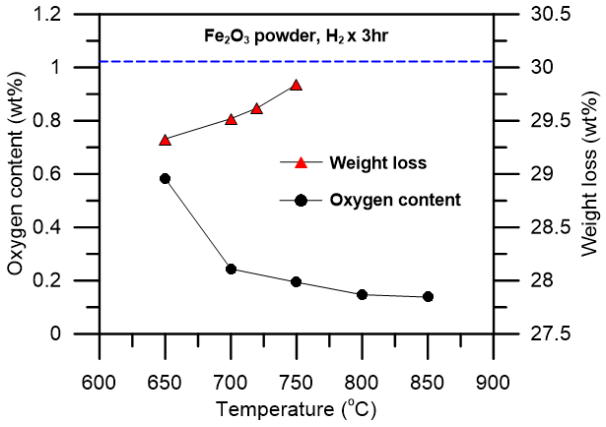

Fig.3. The changes in oxygen content and weight loss of oxide powder at different reaction temperatures.

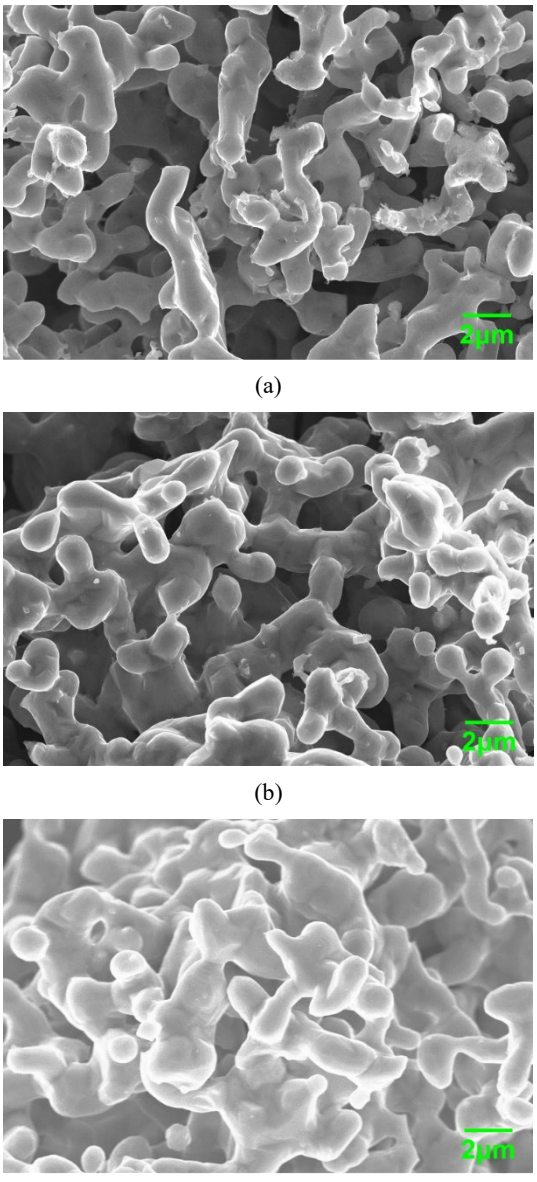

(a)

(b)

(c)

Fig.4. Morphologies of the iron oxide powder after reduction at various temperatures. (a) 650°C, (b) 750°C, (c) 850°C.

Figure 5 illustrates the correlation between particle size and tap density of FRIP powders acquired through the MPS treatment of ACM for different reduced iron agglomerates at various reduction temperatures. As the reduction temperature decreases, the degree of sintering is less pronounced, making it easier to pulverize. Therefore, the particle size after ACM treatment was smaller, but the tap density was also lower. On the contrary, when the reduction temperature was higher, the degree of sintering neck formation increased. This condition is not conducive to the pulverizing and refining of the iron agglomerates, resulting in larger particle sizes and higher tap density. The results were consistent with previous literature[8]. Under the optimal conditions of ACM in this study, the tap density of iron powder with a D50 particle size of about 10 μm could reach 4.04 g/cm³. However, with the current MPS method and ACM conditions, it is quite challenging to produce iron powder that can achieve a D50 particle size smaller than 6 μm while maintaining a tap density of over 4 μm, similar to CIP.

To enhance the tap density of FRIP further, the SGC method was utilized to coat silica on the surface of FRIP.

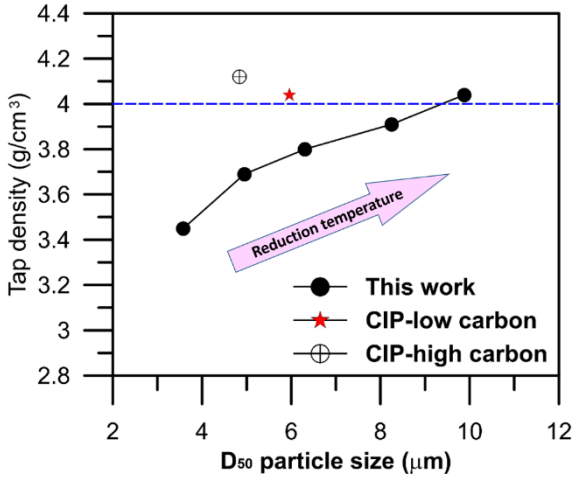

Fig.5. Comparison of D_{50} particle size and tap density of FRIP obtained after MPS treatment of the reduced iron agglomerates at various reduction temperatures.

Figure 6 displays the surface morphologies of FRIP before and after SGC treatment. Numerous nano-silica particles were evenly dispersed on the surface of FRIP using the sol-gel method. However, further TEM/EDS analysis, as shown in Figure 7, illustrates that the FRIP powder surface was covered with a continuously thin-film layer of nanoparticles, not discrete. The thickness of the continuous film layer was about 20 nm, and the total silicon content of the FRIP after SGC treatment increased from 0.008 % to 0.1 %, as confirmed by ICP analysis. Table 2 shows the powder characteristics of the FRIP with and without SGC treatment, and compares them with two commercial CIP powders. It can be seen that the overall particle size of FRIP before and after

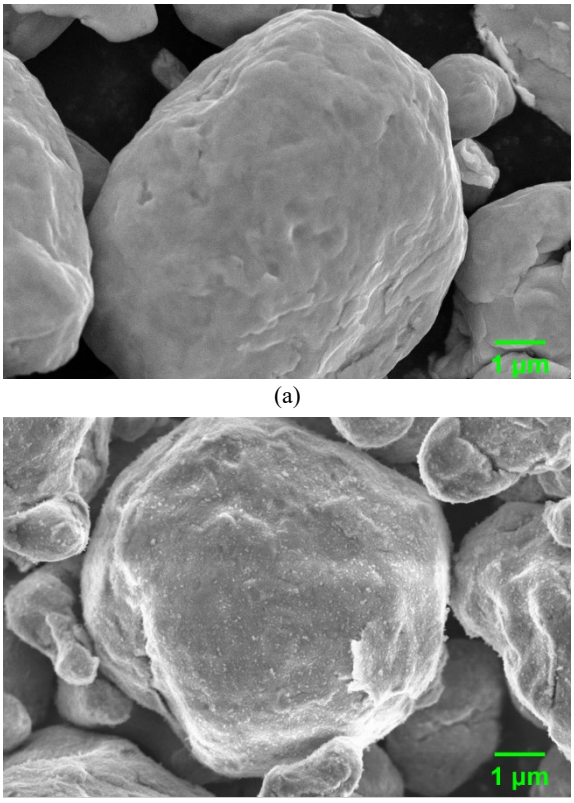

(a)

(b)

Fig.6. Surface morphology of FRIP obtained (a) before and (b) after the MPS treatment.

Table 2 Characteristics of FRIP powders and a comparison with two CIP powders used in MIM.

Iron powder	Particle size (μm) D10 / D50 / D90	Tap density (g/cm³)	BET (m²/g)	Impurity (wt%) C / O / N
FRIP	2.24 / 4.97 / 11.19	3.73	0.466	0.003 / 0.583 / 0.003
Silica-coated FRIP	2.69 / 5.11 / 10.05	4.21	0.824	0.005 / 0.856 / 0.003
CIP-low carbon	3.08 / 5.96 / 9.88	4.04	0.309	0.006 / 0.315 / 0.011
CIP-high carbon	2.47 / 4.84 / 7.64	4.12	0.375	0.792 / 0.435 / 0.643

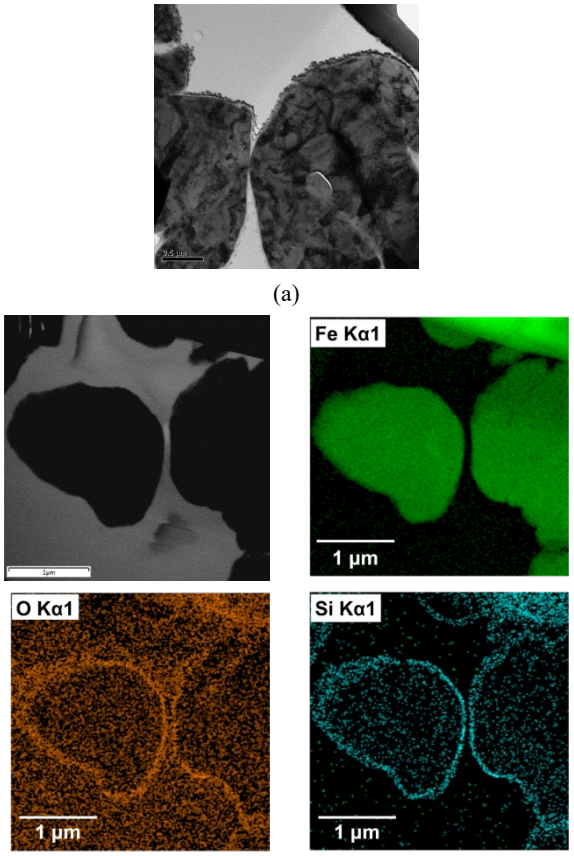

Fig.7. (a) TEM image and (b) EDS mappings of FRIP after the SGC treatment.

silica coating was similar, but the tap density increased significantly from 3.73 g/cm³ to 4.21 g/cm³. Due to the abundance of nanoparticles on the surface of the silica-coated FRIP, the SSA and oxygen content also increased significantly. Moreover, through the SGC treatment, the particle size of the FRIP is close to that of commercial carbonyl iron powders, and its tap density is comparable to them, even slightly higher. Figure 8 illustrates the microstructure evolution at each stage of producing FRIP with high tap density. It reveals that submicron Fe_2O_3 powders were transformed into coarse iron agglomerates through a reduction reaction with hydrogen, and pre-sintering occurred simultaneously. Further mechanical pulverizing and spheroidizing steps refined the iron agglomerates into nearly spherical fine iron powder. Furthermore, the surface modification involving the introduction of a nano-silica coating step provided the iron powders with a nanoscale roughness, consequently reducing the adhesion forces between the iron powder particles. This enhancement improved their fluidity and tap density. Thus, we successfully obtained new iron powders whose properties closely resemble those of CIP for use in MIM.

3.2 Availability evaluation of FRIP for use in the MIM industry

To evaluate the feasibility of applying the FRIP to the MIM process, both non-coated and silica-coated FRIP were mixed with 2% Ni powders and kneaded with polymer binders to prepare Fe-2Ni feedstocks. Figure 9

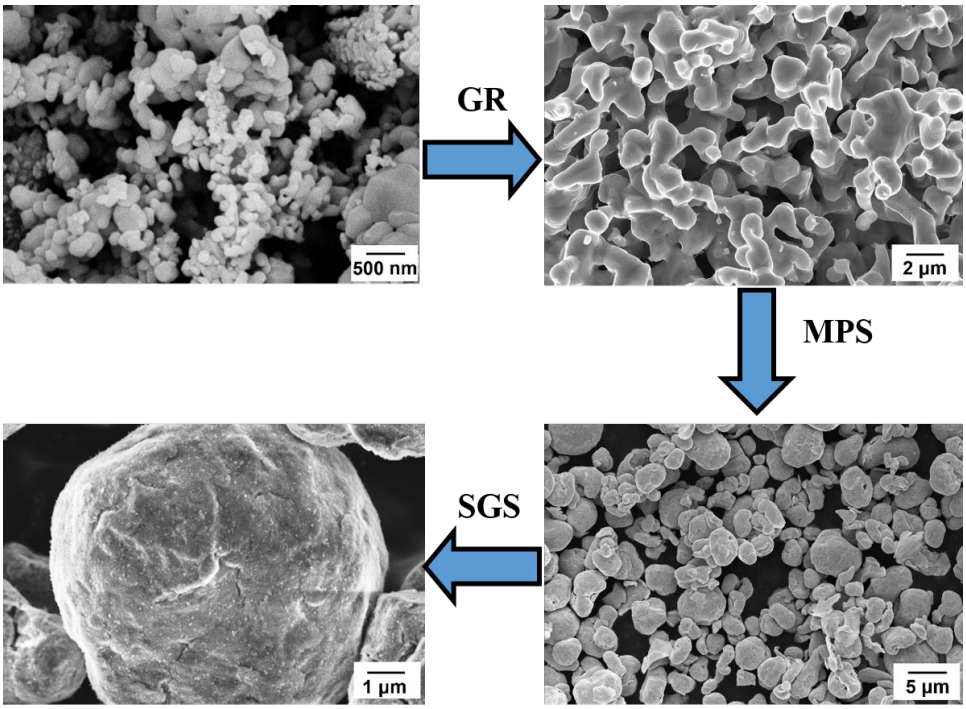

Fig.8. Illustration of the microstructure evolutions at each stage for producing FRIP with high tap density.

compares the dough appearance of the two types of FRIP after kneading with a binder at 7 wt% and 9 wt% of binder content, respectively. When the non-silica coated FRIP was mixed with 7 wt% binder, which is a typically adopted amount for CIP in the MIM industry, the kneading behavior appeared to exhibit higher viscosity, poorer fluidity, and more parched during the compounding of the feedstock. Consequently, the final dough ability was relatively poor. This indicates that the amount of polymer was insufficient to evenly cover the surface of the powder during the kneading process. It was not until the binder content was increased to 9 % that the kneading behavior of the non-silica-coated FRIP improved, and the doughability became better. On the contrary, the silica-coated FRIP only needed to add 7 wt% binder to exhibit good kneading behavior and doughability. With a 9 wt% binder addition, the kneading behavior improved further. Since the surface-treated FRIP exhibited more desirable rheological properties than those of non-treated FRIP, the Fe-2Ni feedstock with 7wt% polymers was further used for injection molding.

Figure 10 shows the appearance of the molded parts of the FRIP feedstock after solvent debinding and thermal debinding. No defects were observed in the appearance of all parts. After sintering, the sintered properties of the Fe-2Ni alloy for FRIP were compared with those of two commercial CIPs, as listed in Table 3. It can be observed that the carbon (C), nitrogen (N), and oxygen (O) content of Fe-2Ni alloys, produced from three distinct iron powders and sintered in hydrogen, were all relatively low and consistent, although the initial CIP-high carbon showed higher carbon content (0.792 wt%) and nitrogen content (0.643 wt%). However, the sintered density of the Fe-2Ni alloy produced by the FRIP reached 7.66 g/cm³, which was higher than the 7.59 g/cm³ of the CIP-high carbon and 7.52 g/cm³ of the CIP-low carbon. Comparing the optical micrographs of the three sintered Fe-2Ni alloys shown in Figure 11 reveals that the number of pores was consistent with the results of the sintered density measured by Archimedes' method. This indicates that the FRIP exhibited better

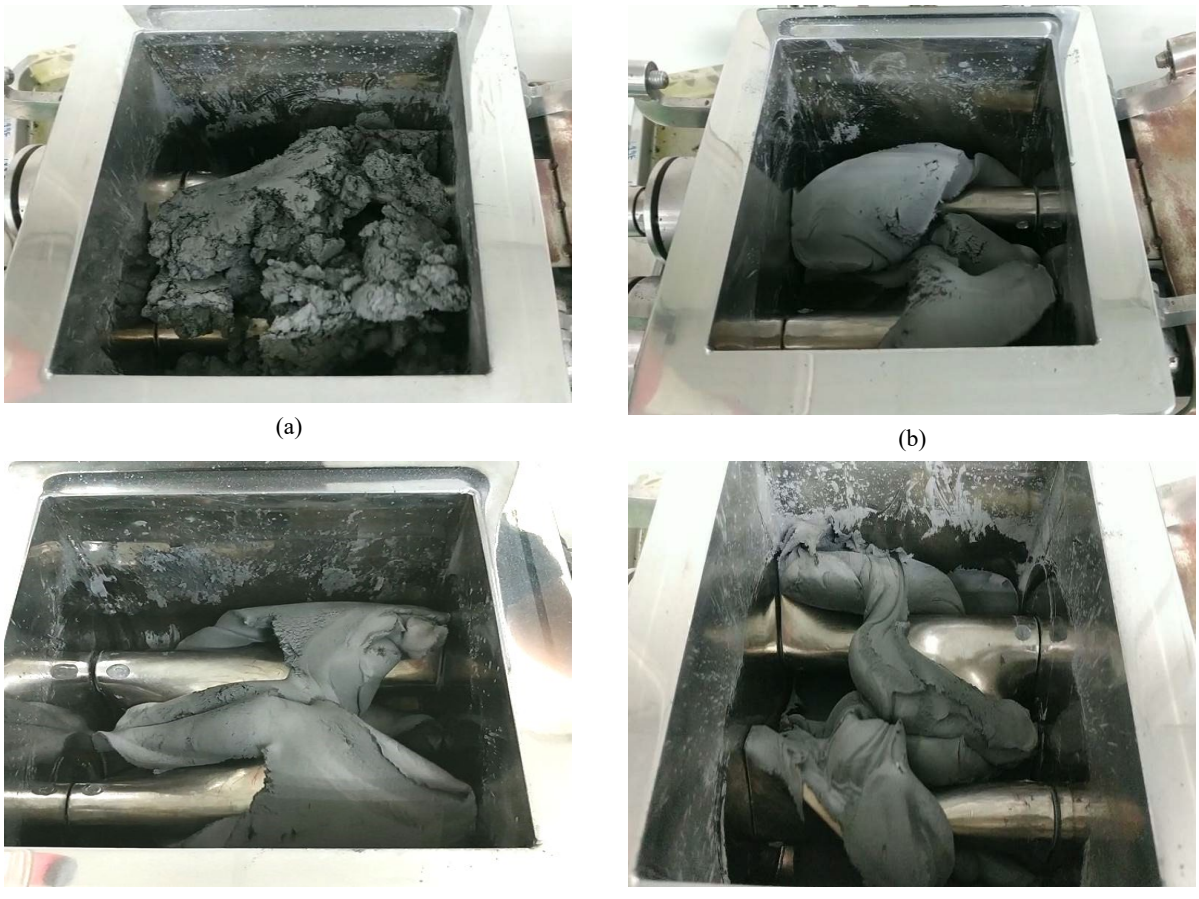

(a) (b) (c) (d)

Fig.9. Comparison of the dough appearance of Fe-2Ni feedstock obtained at different preparing conditions. (a) non-silica coated FRIP, 7 wt% binder, (b) non-silica coated FRIP, 9 wt% binder, (c) silica-coated FRIP, 7 wt% binder, (d) silica-coated FRIP, 9 wt% binder.

Fig.10. Surface condition of the molded parts after solvent debinding and thermal debinding. No defects can be found in any molded parts.

sintering activity than the commercial CIP. This may be attributed to the fact that the specific surface area of the FRIP is higher than that of CIP at the same level of particle sizes, as shown in Table 2. Moreover, since the sintered density of the FRIP was higher, the hardness of the FRIP was also slightly higher than that of the two CIP powders. In addition, although the shrinkage of the sintered compacts made by the FRIP was the largest among the three iron powders, its standard deviation was the best. This may be attributed to the fact that the shape of FRIP is not as completely spherical as that of CIP powder. Thus, there is relatively higher friction between the powders, enhancing the mechanical interlocking effect. This makes it less likely to deform during the debinding process, ultimately benefiting dimensional stability control during sintering. In terms of the overall properties of Fe-2Ni, the properties of the Fe-2Ni alloy made from FRIP powder were also comparable to the MPIF standard. Based on the absence of any issues with using FRIP in the MIM process, and the sintered properties being equivalent to MPIF standards, it is evident that our developed FRIP has high potential for use in the MIM industry.

4. CONCLUSIONS

Based on the established gaseous reduction (GR), mechanically pulverized and spheroidized (MPS), and sol-gel coating (SGC) technologies, finely reduced iron powder (FRIP) can be produced for use in the MIM industry. This study found that the reduction temperature and the SGC treatment significantly affect the powder properties of iron powder. Through the optimization of the GR+MPS+SGC process, the particle size and tap density of the iron powder can be achieved at a level comparable to that of commercial carbonyl iron powder. During the Metal Injection Molding (MIM) process evaluation, silica-coated FRIP, nickel powder, and binder can be effectively mixed into a Fe-2Ni alloy feedstock. After injection, debinding, and sintering, the sintered density of the Fe-2Ni reached 7.66 g/cm³, and the standard deviation of the dimensional changes of the MIM compacts is 0.01, both of which were slightly better than those of commercial CIP benchmark products. Although all results indicate that FRIP has the potential to be used in the MIM industry, it still needs to be verified through actual use by downstream MIM manufacturers.

Table 3 Comparison of properties for Fe-2Ni alloy prepared by the surface-coated FRIP and two CIP powders.

	Properties of Fe-2Ni alloy										
Iron powder used	C (wt%)	O (wt%)	N (wt%)	Hardness (HRB)	Sintered density (g/cm³)	Length of sintered compact			Width of sintered compact		
						AVG (mm)	STD	Shrinkage rate (%)	AVG (mm)	STD	Shrinkage rate (%)
CIP-low carbon	0.004	0.004	0.009	50	7.52	25.69	0.05	14.35	8.56	0.02	14.36
CIP-high carbon	0.008	0.004	0.010	53	7.59	25.61	0.03	14.63	8.54	0.01	14.64
FRIP (surface coated)	0.008	0.003	0.010	57	7.66	25.52	0.01	14.91	8.51	0.01	14.92
MIM-2200 MPIF Standard (typical)	0.1 max	-	-	45	7.65	-	-	-	-	-	-

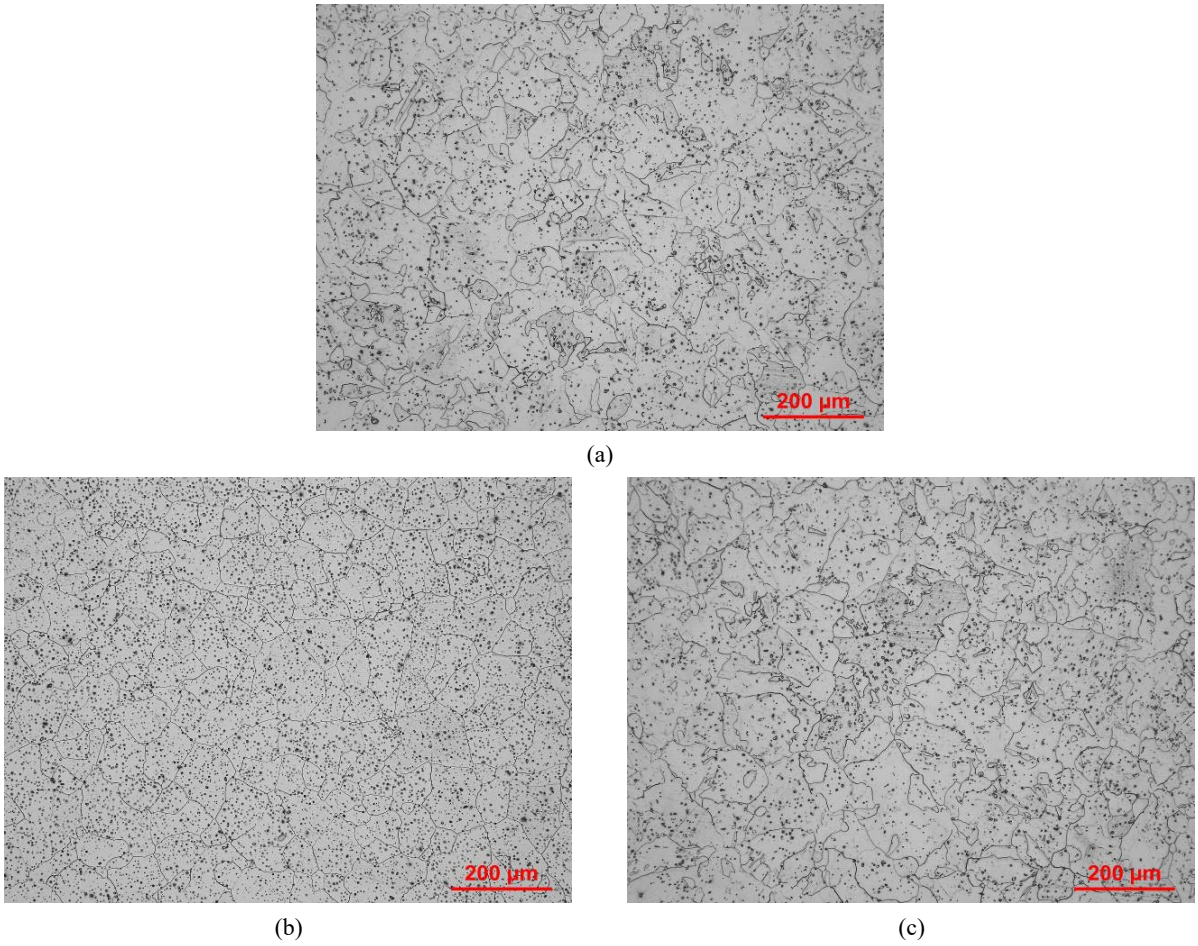

Fig.11. Comparison of microstructures for Fe-2Ni steel prepared by (a) silica-coated FRIP, (b) CIP-low carbon, and (c) CIP-high carbon.

REFERENCES

1. J. Shu and L. Koehler: Powder Metall. Rev., 2017, vol. 6, pp. 39-49.
2. D. Bloemacher: Met. Powder Rep., 1990, vol. 45, pp. 117-119.
3. A. Alghtani, M. Alsharef, and K. A. El-Aziz: Mater. Res., 2022, vol. 25, pp. 1-11.
4. D. W. Clark and C. W. Cornelssen: United States Patent No. 6,569,220 B1.
5. G. Walther, T. Büttner, B. Kieback, T. Weißgärber, M. Hoffmann, and G. Bachmann: J. Powder Metal., 2014, vol. 57, pp. 176-183.
6. G. Walther, T. Büttner, B. Kieback, T. Weißgärber, and M. Hoffmann: "Manufacturing of Fine Spherical Iron Powder and the Influence of the Powder Morphology on the Sintering Behaviour" in Proc. World PM2016, Hamburg, Germany, Oct. 9-13, 2016.
7. A. Böhm, T. Büttner, T. Weißgärber, B. Kieback and W. Pieper: "Particle Modification and Powder Design using the NARA Hybridizer"; pp. 131-135 in Proc. World PM2004, Vienna, Austria, Oct. 17-21, 2004.
8. C. Y. Chen: Process and Properties of Fine Reduced Iron Powder, Master Thesis of National Taiwan University, Taipei, Taiwan, 2009, pp. 49-86.
9. Y. Li, L. Li and K. A. Khalil: J. Mater. Process. Technol., 2007, vol. 183, pp. 432-439.
10. R. Sharma and G. Setia: Powder Technol., 2019, vol. 356, pp. 458-479.
11. Y. Chen, J. Yang, R.N. Dave and R. Pfeffer: AIChE J., 2008, vol. 54, pp. 104-121.
12. Y. Zhou and J. Zhu: Powder Technol., 2021, vol. 381, pp. 698-720.
13. P. Małecki, K.Kolman, J.Pigłowski, J.Kaleta, and J.Krzak: J. Solid State Chem., 2015, vol. 226, pp. 224-230.